

14



ETMM

Ercoftac Symposium on
Engineering Turbulence
Modelling and Measurements

6th - 8th September 2023
Barcelona, Spain



14th International ERCOFTAC Symposium on Engineering Turbulence Modelling and Measurements

PROCEEDINGS



HOT-WIRE SPATIAL RESOLUTION EFFECTS IN ADVERSE-PRESSURE-GRADIENT TURBULENT BOUNDARY LAYERS

*Artur Drózdź¹, Ramis Örlü^{2,3}, Paweł Niegodajew¹,
Vasyl Sokolenko¹, Philipp Schlatter^{2,4} and Witold Elsner¹*

¹ *Czestochowa University of Technology, Department of Thermal Machinery
al. Armii Krajowej 21, 42-200 Czestochowa, Poland*

² *SimEx, Engineering Mechanics, KTH Royal Institute of Technology
SE-100 44 Stockholm, Sweden*

³ *Department of Mechanical, Electronic and Chemical Engineering
OsloMet – Oslo Metropolitan University, 0166 Oslo, Norway*

⁴ *Institute of Fluid Mechanics (LSTM)
Friedrich-Alexander-Universität (FAU) Erlangen-Nürnberg, Germany*

artur.drozd@pcz.pl

Abstract

The effect of a finite length hot-wire sensor on the measured streamwise velocity fluctuations is well understood in canonical wall-bounded flow. In particular, the small-scale energy has been found to be universal among canonical flows and invariant with Reynolds number and has therefore been exploited in correction schemes for attenuated measurements. A straightforward application to non-canonical flows such as strong adverse pressure gradient (APG) flows has, however, been hampered since the effect of Reynolds number and pressure gradient conditions could not be studied separately due to the lack of data with a clear scale separation. The present experimental investigation at a fixed friction Reynolds number of around 4000 in weak, moderate and strong APG conditions with different wire lengths shows that while spatial averaging effects are not only limited to the inner layer but extend also into the outer layer, their influence on both layers diminishes for strong pressure gradient conditions. A note of caution is hence warranted for measurements that seemingly try to take the bias effect of spatial attenuation into account by performing measurements with albeit long but fixed viscous-scaled wire lengths.

1 Introduction

The effect of spatial averaging in the measurement of small-scale turbulence energy appears to be well understood in zero-pressure-gradient (ZPG) turbulent boundary layers (TBL) [1]. Particularly, it is well known how hot-wire measurements taken with varying viscous-scaled wire lengths l^+ , tend to mask true Reynolds number effects [2, 3]. It was e.g., thought

that the outer peak in the streamwise variance profile in ZPG TBLs emerges with increasing Re already at moderate Re . However, well-resolved turbulence measurements showed at these Re [4], that this effect was an artefact of insufficient spatial resolution that attenuates the small-scale energy near the wall [5]. In fact, compelling evidence from ZPG TBLs but also other canonical wall-bounded flows has shown, that the small-scale energy is universal, i.e. independent of Reynolds number [6], which in turn opened doors to model the near-wall region by superimposing large-scale information from the outer layer onto the *a priori* known universal small-scale signal [7]. While these observations have been made across various canonical wall-bounded flows, there are several observations in non-canonical flows that challenge the notion of small-scale universality. As such, the small-scale energy related near-wall peak ($y^+ \approx 15$) is apparently weaker in adverse-pressure-gradient (APG) TBL [8], while at the same time the outer peak in light of the energized large-scale motions increases to a greater extent compared to ZPG TBLs [9]. Similarly, there are indications that the small-scale energy is shifted towards larger scales [10], thereby inhibiting the utilization of models based on the universal small-scale energy both for modelling but also spatial resolution corrections methods for measurement techniques [10]. Most of these studies are, however, inconclusive, due to the difficulty to clearly distinguish between small and large scales since either the numerical data exhibiting strong APG conditions are limited to low Reynolds numbers or experimental studies at higher Reynolds numbers are (usually) limited to weak APG conditions.

The present work aims at further investigating the importance of spatial averaging effects in measure-

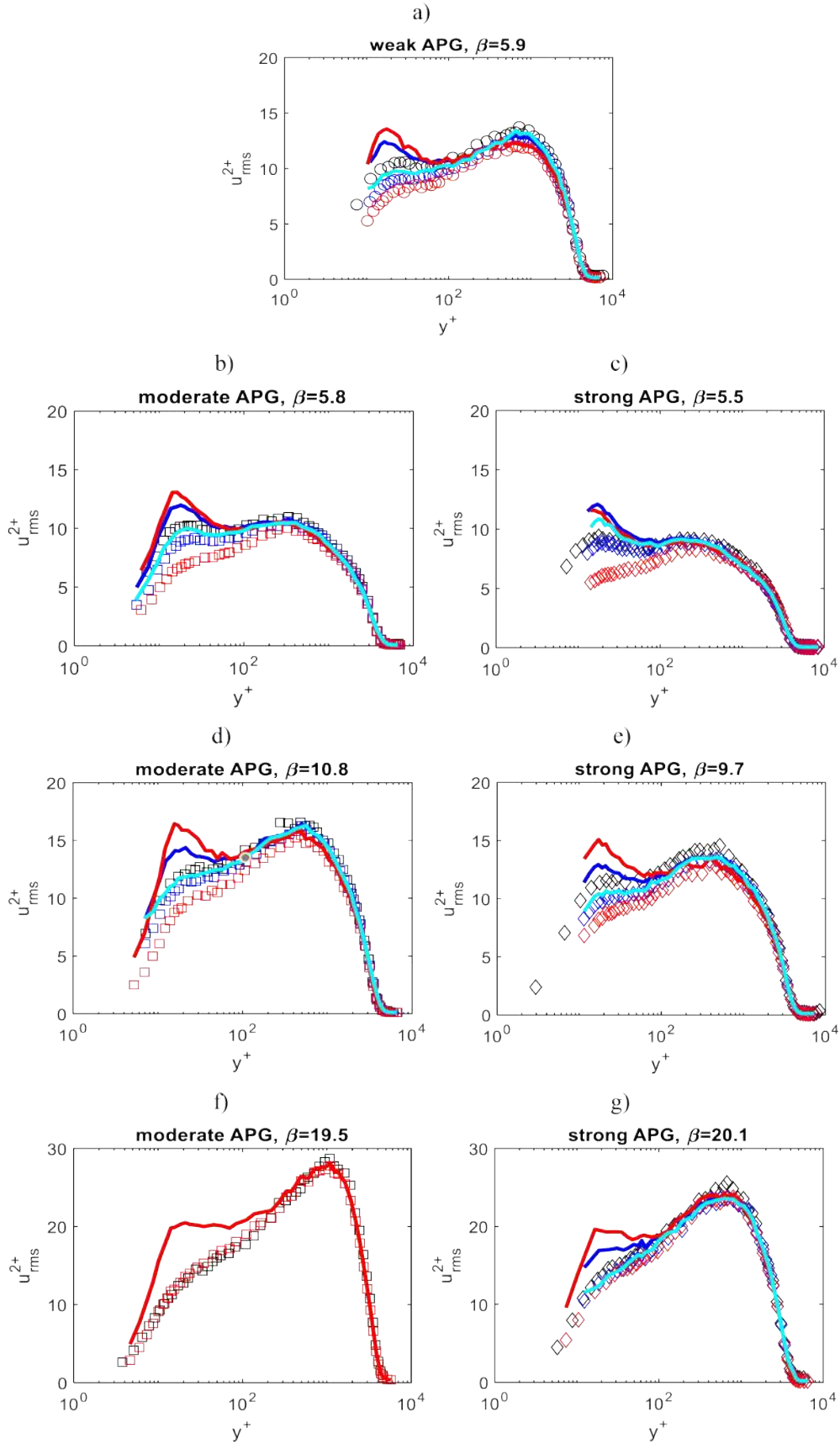


Figure 3: Effect of hot-wire spatial averaging on streamwise Reynolds normal stress for $\beta \approx 5.7$ (a - weak APG, b - moderate APG and c - strong APG), $\beta \approx 10$ (d - moderate APG, e - strong APG) and $\beta \approx 20$ (f - moderate APG and g - strong APG). Dark symbols: $l = 0.41$ mm; blue symbols: $l = 1.25$ mm; red symbols $l = 3.0$ mm, Blue line: Smits $l = 1.25$ mm; red line: Smits $l = 3.0$ mm; Cyan line: Segalini $l = 1.25$ mm & $l = 3.0$ mm

in line with the assumption that the flow adapts to the cumulative effect of β rather than to its local value, cf. Refs. [11, 12]. Also when a flow exhibits a strong pressure gradient it can adapt to a local gradient of the pressure coefficient $\delta_{in}dC_P/dx$ which was shown in diagnostic plot scaling of the turbulence intensity profile introduced by Drózdź *et al.* [13]. It can be noticed that the C_P distribution is the same up to $x = 500$ mm from the ZPG inlet (see Fig. 2).

Figure 3 depicts a compilation of plots of the inner-scaled streamwise variance profiles for various pressure gradient conditions. The measured values with different hot-wire lengths are indicated through colored symbols. Dark symbols: $l = 0.41$ mm; blue symbols: $l = 1.25$ mm; red symbols $l = 3.0$ mm. The results for the considered range of l^+ values show that spatial averaging in APG TBLs is complex and not restricted to the inner layer only since small-scale-energy attenuation is also visible in the outer layer.

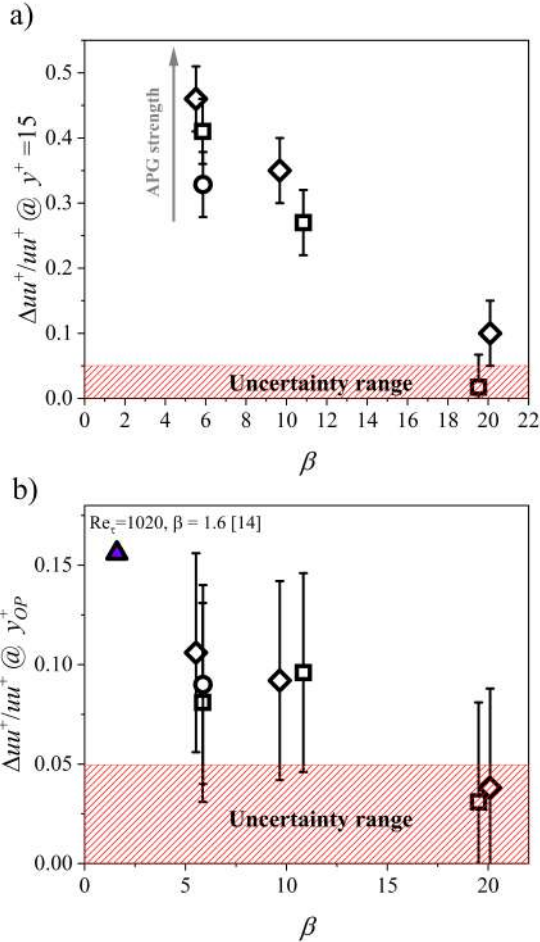


Figure 4: Effect of hot-wire spatial averaging on streamwise Reynolds normal stress maxima with β at inner peak a) and at outer peak b). Uncertainty level 5.0%. The triangle symbol represents the data from Ref. [14]

Figure 3 shows that the effect of spatial averaging weakens with increasing local β , i.e., there are clear differences between the profiles measured with different wire lengths especially for β values of 5 and 10. The effect of wire length diminishes for $\beta \approx 20$. This observation indicates a clear bias towards large-scale energy compared to small-scale energy (where small in this case denotes scales smaller than the wire length). This observation is in line with the recent finding of Deshpande *et al.* [14].

When comparing different APGs one should observe that the weak APG case at $\beta \approx 5.9$ (Fig. 3a) is similar to the strong APG case at $\beta \approx 9.7$ (Fig. 3e) in terms of near-wall and outer peaks levels. It can be concluded that with the increase of APG strength the outer peak weakens for the same β values. It is in line with the conclusions of Bobke *et al.* [11] and Sanmiguel Vila *et al.* [15] who noted, from observing the viscous-scaled mean statistics, that flows with increas-

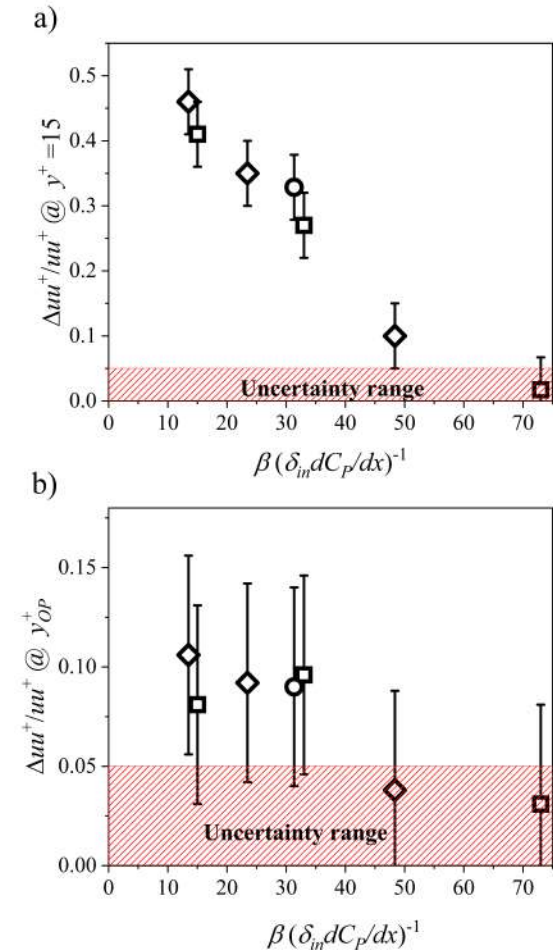


Figure 5: Effect of hot-wire spatial averaging on streamwise Reynolds normal stress maxima with $\beta / (\delta_{in} dC_P/dx)$ at inner peak a) and at outer peak b). Uncertainty level 5.0%

ing β exhibit behaviors akin to those at much smaller β , and thus retain the character of the upstream condition. The attenuated energy is at a similar level for those cases which may indicate a similar small-scale energy content at different local β .

To investigate the effect of spatial averaging and the associated attenuation of small-scale energy in more detail it is helpful to consider the difference in amplitude of the streamwise variance profile for both the inner and outer peaks. Fig. 4 depicts the percentage in difference between the profiles measured with the shortest and longest probe for all β evolution as a function of local β . A clear decay of the effect of attenuation at the location of the inner-peak is apparent, from nearly 50% attenuation for the low value of β down to below 10% at a high value of β . This drastic decrease is related to the dominance of small-scale energy around the near-wall cycle. The level of attenuation at the location of the outer peak is clearly less pronounced to start with, but also here, an increase of β brings a clear decrease of the effect of attenuation with it; with values diminishing within the uncertainty of the measurements. It is hence clear that small-scale energy becomes less dominant throughout the entire boundary layer with increasing local β , thereby underlining the transition of a wall-dominated flow towards a wake-dominated flow. For comparison also one data point from the study of Deshpande *et al.* [14] at a lower local β is shown confirming the trend of the present data. It is interesting to note that this implies that with increasing APG strength (increase in dC_P/dx), spatial resolution issues become more important.

Figure 5 presents the same data as in Fig. 4, however as a function of $\beta/(\delta_{in}dC_P/dx)$. As can be seen, the data in such a presentation form becomes even more arranged and the decaying trend of attenuation with increasing $\beta/(\delta_{in}dC_P/dx)$ is even more severe for both inner and outer peak when compared to the one from Fig. 4.

To quantify the attenuated energy of small scales in the inner and outer layer separately for the moderate APG $\beta = 5.8$ case, the iso-contours of the wavelet energy spectra E (equivalent to pre-multiplied energy spectra), scaled by the friction velocity u_τ , are presented in Fig. 6 as a function of the normalised time scale τ^+ and normalised wall distance y^+ . As shown in Ref. [16], the convection velocity distribution is universal in the inner region of TBL. Therefore, the convection velocity was used to show the streamwise spatial scale $\lambda^+ = 4000$ (red line) which splits the wavelet energy spectra into regions with small and large scales (values of τ^+ below and above that line), respectively. It confirms that the small scales energy is attenuated for both near-wall and outer region.

Turning now to the correction schemes, and considering the one introduced by Smits *et al.* [17], which per definition is only valid in canonical flows in which small-scale universality holds. A straightforward

application of their correction regardless of range of applicability, is given through the solid lines in Fig. 3. As can be anticipated, there is an apparent overestimation of the variance profiles in the inner layer, due to shift of energy from small to large scales with increasing APG strengths. A method that might not be limited to cases in which the universality of the small-scale energy is a prerequisite is the method by Segalini *et al.* [18] which is also shown in Fig. 3. This method clearly performs better in the inner layer, since it relies on the information from two measured attenuated profiles; which is also the method's drawback compared to other methods requiring only one profile.

4 Conclusions

This paper explores the effect of hot-wire sensor length on the measured streamwise velocity fluctuations at a fixed friction Reynolds number of around 4000 under weak, moderate and strong APG conditions. The results show that spatial averaging effects that takes place due to attenuation of small scale energy are not limited to the inner layer, but extent also into the outer layer. The influence of wire length (for the considered range of wire lengths) in both layers reduces for strong pressure gradient conditions when β reaches ≈ 20 . In general, in terms of flow history, with growing APG strength for the same β values the attenuation becomes stronger which indicates that the share of the small-scale

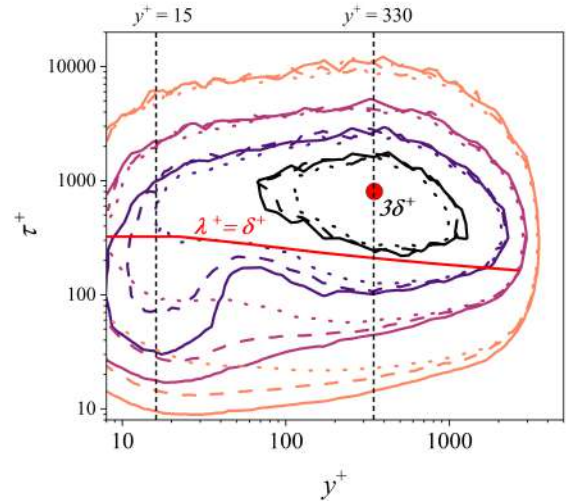


Figure 6: Effect of hot-wire spatial averaging on inner scaled streamwise pre-multiplied time-scale spectra for moderate APG $\beta = 5.7$. The red line corresponds to streamwise spatial scale $\lambda^+ = 4000$ where the convection velocity was used instead of mean velocity. Continuous line $l = 0.41$ mm, dashed line $l = 1.25$ mm and dotted line $l = 3.0$ mm. Increments between level equals 0.5.

energy also increases in the flow. Interestingly, the correction scheme of Segalini *et al.* [18] performs well in reproducing both inner and outer peaks for the investigated cases since it does not rely on universality of small-scale structures.

Acknowledgments

The investigation was supported by National Science Centre under Grant No. DEC-2020/39/B/ST8/01449.

References

- [1] N. Hutchins, T. B. Nickels, I. Marusic, and M. S. Chong. Hot-wire spatial resolution issues in wall-bounded turbulence. *J. Fluid Mech.*, 635:103–136, 2009.
- [2] M. Metzger. Length and time scales of the near-surface axial velocity in a high Reynolds number turbulent boundary layer. *Int. J. Heat Fluid Flow*, 27(4):534–541, 2006.
- [3] R. Örlü and P. H. Alfredsson. On spatial resolution issues related to time-averaged quantities using hot-wire anemometry. *Exp. Fluids*, 49:101–110, 2010.
- [4] M. Samie, I. Marusic, N. Hutchins, M. K. Fu, Y. Fan, M. Hultmark, and A. J. Smits. Fully resolved measurements of turbulent boundary layer flows up to $Re_\tau=20000$. *J. Fluid Mech.*, 851:391–415, 2018.
- [5] P. H. Alfredsson, A. Segalini, and R. Örlü. A new scaling for the streamwise turbulence intensity in wall-bounded turbulent flows and what it tells us about the ‘outer’ peak. *Phys. Fluids*, 23:041702, 2011.
- [6] I. Marusic, B. J. McKeon, P. A. Monkewitz, H. M. Nagib, A. J. Smits, and K. R. Sreenivasan. Wall-bounded turbulent flows at high reynolds numbers: Recent advances and key issues. *Phys. Fluids*, 22(6), 2010.
- [7] I. Marusic, R. Mathis, and N. Hutchins. Predictive model for wall-bounded turbulent flow. *Science*, 329(5988):193–196, 2010.
- [8] A. Drózdź, P. Niegodajew, M. Romańczyk, and W. Elsner. Effect of Reynolds number on turbulent boundary layer approaching separation. *Exp. Thermal Fluid Sci.*, 125:110377, 2021.
- [9] P. Niegodajew, A. Drózdź, and W. Elsner. A new approach for estimation of the skin friction in turbulent boundary layer under the adverse pressure gradient conditions. *Int. J. Heat Fluid Flow*, 79:108456, 2019.
- [10] C. Sanmiguel Vila, R. Vinuesa, S. Discetti, A. Ianiro, P. Schlatter, and R. Örlü. Separating adverse-pressure-gradient and Reynolds-number effects in turbulent boundary layers. *Phys. Rev. Fluids*, 5:064609, 2020.
- [11] A. Bobke, R. Vinuesa, R. Örlü, and P. Schlatter. History effects and near-equilibrium in adverse-pressure-gradient turbulent boundary layers. *J. Fluid Mech.*, 820:667–692, 2017.
- [12] R. Vinuesa, R. Örlü, C. Sanmiguel Vila, A. Ianiro, S. Discetti, and P. Schlatter. Revisiting history effects in adverse-pressure-gradient turbulent boundary layers. *Flow, Turbul. Combust.*, 99:565–587, 2017.
- [13] A. Drózdź, P. Niegodajew, W. Elsner, R. Vinuesa, R. Örlü, and P. Schlatter. A description of turbulence intensity profiles for boundary layers with adverse pressure gradient. *European Journal of Mechanics - B/Fluids*, 84:470–477, nov 2020.
- [14] R. Deshpande, A. van den Bogaard, R. Vinuesa, L. Lindić, and I. Marusic. Reynolds-number effects on the outer region of adverse-pressure-gradient turbulent boundary layers. *arXiv preprint arXiv:2304.08714*, 2023.
- [15] C. Sanmiguel Vila, R. Örlü, R. Vinuesa, P. Schlatter, A. Ianiro, and S. Discetti. Adverse-pressure-gradient effects on turbulent boundary layers: statistics and flow-field organization. *Flow Turbul. Combust.*, 99:589–612, 2017.
- [16] A. Drózdź, P. Niegodajew, M. Romańczyk, and W. Elsner. Convection velocity in turbulent boundary layers under adverse pressure gradient. *Experimental Thermal and Fluid Science*, 145C:110900, 2023.
- [17] A. J. Smits, J. Monty, M. Hultmark, S. C. C. Bailey, N. Hutchins, and I. Marusic. Spatial resolution correction for wall-bounded turbulence measurements. *J. Fluid Mech.*, 676:41–53, 2011.
- [18] A. Segalini, R. Örlü, P. Schlatter, P. H. Alfredsson, J.-D. Rüedi, and A. Talamelli. A method to estimate turbulence intensity and transverse Taylor microscale in turbulent flows from spatially averaged hot-wire data. *Exp. Fluids*, 51:693, 2011.